Draft version October 31, 2014
Preprint typeset using LaTeX style emulateapj v. 05/12/14

RED SUPERGIANT STARS AS COSMIC ABUNDANCE PROBES: KMOS OBSERVATIONS IN NGC 6822

L. R. Patrick[1], C. J. Evans[2,1], B. Davies[3], R-P. Kudritzki[4,5], J. Z. Gazak[4], M. Bergemann[6], B. Plez[7], A. M. N. Ferguson[1]

Draft version October 31, 2014

ABSTRACT

We present near-IR spectroscopy of red supergiant (RSG) stars in NGC 6822, obtained with the new VLT-KMOS instrument. From comparisons with model spectra in the J-band we determine the metallicity of 11 RSGs, finding a mean value of $[\mathrm{Z}] = -0.52 \pm 0.21$ which agrees well with previous abundance studies of young stars and HII regions. We also find an indication for an abundance gradient within the central 1 kpc, although with low significance because of the small number of objects studied. We compare our results to those derived from older stellar populations and investigate the difference using chemical evolution models. By comparing the physical properties determined for RSGs in NGC 6822 with those derived using the same technique in the Galaxy and the Magellanic Clouds, we show that there appears to be no significant temperature variation of RSGs with respect to metallicity, in contrast to recent evolutionary models.

Keywords: Galaxies: individual: NGC 6822 – stars: abundances – stars: supergiants

1. INTRODUCTION

A promising new method to directly probe chemical abundances in external galaxies is with J-band spectroscopy of red supergiant (RSG) stars. With their peak flux at $\sim 1\,\mu$m and luminosities in excess of $10^4\,\mathrm{L}_\odot$, RSGs are extremely bright in the near-IR (with $-8 \leq \mathrm{M}_J \leq -11$). Therefore, RSGs are useful tools with which to map the chemical evolution of their host galaxies, out to large distances. To realise this goal, Davies et al. (2010) outlined a technique to derive metallicities of RSGs at moderate spectral resolving power ($R \sim$3000). This technique has recently been refined using observations of RSGs in the Magellanic Clouds (Davies et al. submitted) and Perseus OB-1 (Gazak et al. 2014). Using absorption lines in the J-band from iron, silicon and titanium, one can estimate metallicity ($[\mathrm{Z}] = \log{(\mathrm{Z}/\mathrm{Z}_\odot)}$) as well as other stellar parameters (effective temperature, surface gravity and microturbulence) by fitting synthetic spectra to the observations. Owing to their intrinsic brightness, RSGs are ideal candidates for studies of extragalactic environments in the near-IR.

To make full use of the potential of RSGs for this science, multi-object spectrographs operating in the near-IR on 8-m class telescopes are essential. These instruments allow us to observe a large sample of RSGs in a given galaxy, at a wavelength where RSGs are brightest. In this context, the K-band Multi-Object Spectrograph (KMOS; Sharples et al. 2013) at the Very Large Telescope (VLT), Chile, is a powerful facility. KMOS will enable determination of stellar abundances and radial velocities for RSGs out to distances of 10 Mpc. Further ahead, a near-IR multi-object spectrograph on a 40-m class telescope, combined with the excellent image quality from adaptive optics, will enable abundance estimates for individual stars in galaxies out to tens of Mpc, a significant volume of the local universe containing entire galaxy clusters (Evans et al. 2011).

Here we present KMOS observations of RSGs in the dwarf irregular galaxy NGC 6822, at a distance of $\sim$0.46 Mpc (McConnachie 2012, and references therein). Its present-day iron abundance is thought to be intermediate to that of the LMC and SMC (Kirby et al. 2013), but we lack firmer constraints on both its metallicity and its recent chemical evolution. Observations of two A-type supergiants by Venn et al. (2001) provided a first estimate of stellar abundances, finding log (Fe/H) $+12 = 7.01 \pm 0.22$ and $\log(\mathrm{O/H}) + 12 = 8.36 \pm 0.19$, based on line-formation calculations for these elements, assuming local thermodynamic equilibrium (LTE). A detailed non-LTE study for one of these objects confirmed the results finding 6.96 ± 0.09 for iron and 8.30 ± 0.02 for oxygen (Przybilla 2002). Compared to solar values of 7.50 and 8.69, respectively (Asplund et al. 2009), this indicates abundances that are about 0.5 dex lower in NGC 6822. A study of oxygen abundances in HII regions (Lee et al. 2006) found a value of 8.11 ± 0.1, confirming the low metallicity.

NGC 6822 is a relatively isolated Local Group galaxy, which does not seem to be associated with either M31 or the Milky Way. It appears to have a relatively large extended stellar halo (Letarte et al. 2002; Hwang et al. 2014) as well as an extended HI disk containing tidal arms and a possible HI companion (de Blok & Walter 2000). The HI disk is orientated perpendicular to the distribution of old halo stars and has an associated pop-

[1] Institute for Astronomy, University of Edinburgh, Royal Observatory Edinburgh, Blackford Hill, Edinburgh EH9 3HJ, UK
[2] UK Astronomy Technology Centre, Royal Observatory Edinburgh, Blackford Hill, Edinburgh EH9 3HJ, UK
[3] Astrophysics Research Institute, Liverpool John Moores University, Liverpool Science Park ic2, 146 Brownlow Hill, Liverpool L3 5RF, UK
[4] Institute for Astronomy, University of Hawaii, 2680 Woodlawn Drive, Honolulu, HI, 96822, USA
[5] University Observatory Munich, Scheinerstr. 1, D-81679 Munich, Germany
[6] Institute of Astronomy, University of Cambridge, Madingley Road, Cambridge CB3 0HA, UK
[7] Laboratoire Univers et Particules de Montpellier, Université Montpellier 2, CNRS, F-34095 Montpellier, France

ulation of blue stars (de Blok & Walter 2003; Komiyama et al. 2003). This led Demers et al. (2006) to label the system as a 'polar ring galaxy'. A population of remote star clusters aligned with the elongated old stellar halo have been recently discovered (Hwang et al. 2011; Huxor et al. 2013). The extended structures of NGC 6822 suggest some form of recent interaction.

In addition, there is evidence for a relatively constant star-formation history within the central 5 kpc (Weisz et al. 2014) with multiple stellar populations (Battinelli et al. 2006; Sibbons et al. 2012). This includes evidence for recent star formation in the form of a known population of massive stars, as well as a number of HII regions (Venn et al. 2001; de Blok & Walter 2006; Hernández-Martínez et al. 2009; Levesque & Massey 2012).

In this paper we present near-IR spectroscopy of RSGs in NGC 6822 from KMOS. In Section 2 we describe the observations. Section 3 describes the data reduction and Section 4 details the derived stellar parameters and investigates the presence of an abundance gradient in NGC 6822. In Section 5 we discuss our results and Section 6 concludes the paper.

2. OBSERVATIONS

2.1. *Target Selection*

Our targets were selected from optical photometry (Massey et al. 2007), combined with near-IR (JHK_s) photometry (for details see Sibbons et al. 2012) from the Wide-Field Camera (WFCAM) on the United Kingdom Infra-Red Telescope (UKIRT). The two catalogues were cross-matched and only sources classified as stellar in the photometry for all filters were considered.

Our spectroscopic targets were selected principally based on their optical colours, as defined by Massey (1998) and Levesque & Massey (2012). Figure 1 shows cross-matched stars, with the dividing line at $(B-V) = 1.25 \times (V-R) + 0.45$. All stars redder than this line, with $V - R > 0.6$, are potential RSGs.

To increase confidence in the nature of our targets, those selected using the optical criterion are subjected to an additional criteria based on near-IR photometry, using the known location of RSGs in the $J-K$ colour-magnitude diagram (Nikolaev & Weinberg 2000), as shown in Figure 2.

The combined selection methods yielded 58 potential targets, from which 18 stars were observed with KMOS, as shown in Figure 3. The selection of the final targets was defined by the KMOS arm allocation software KARMA (Wegner & Muschielok 2008), where the field centre was defined to maximise the number of allocated arms, with priority given to the brightest targets. Of the 18 candidates, eight were previously spectroscopically confirmed as RSGs by Levesque & Massey (2012).

2.2. *KMOS Observations*

The observations were obtained as part of the KMOS Science Verification (SV) program on 30 June 2013 (PI: Evans 60.A-9452(A)), with a total exposure time of 2400 s (comprising 8×300 s detector integrations). KMOS has 24 deployable integral-field units (IFUs) each of which covers an area of 2.″8 × 2.″8 within a 7.′2 field-of-view. The 24 IFUs are split into three groups of eight, with the light from each group relayed to different spectrographs.

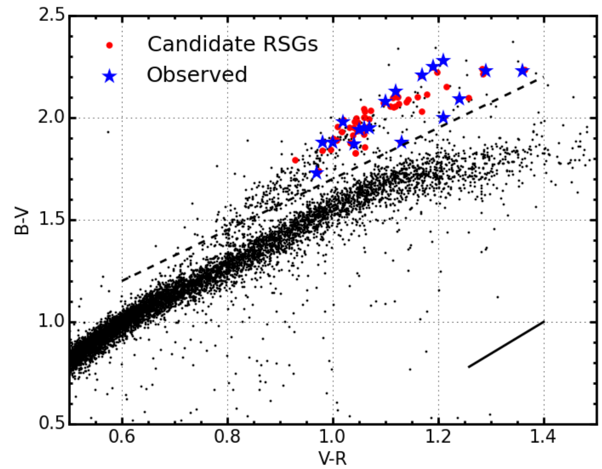

Figure 1. Two-colour diagram for stars with good detections in the optical and near-IR photometry in NGC 6822. The black dashed line marks the selection criteria using optical colours, as defined by Levesque & Massey (2012). Red circles mark all stars which satisfy our selection criteria. Large blue stars denote targets observed with KMOS. The solid black line marks the foreground reddening vector (Schlegel et al. 1998).

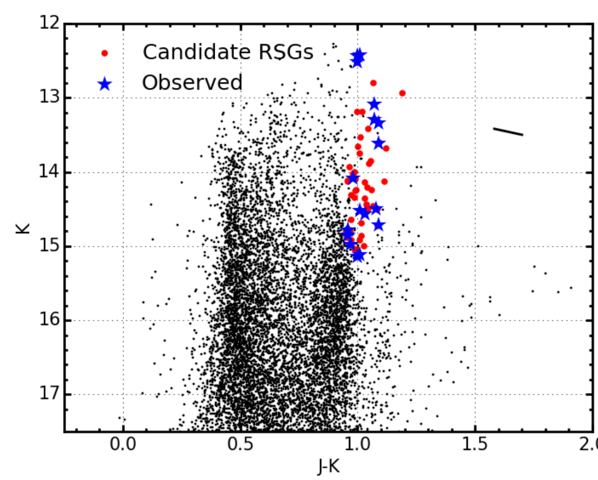

Figure 2. Near-IR colour-magnitude diagram (CMD) for stars classified as stellar sources in the optical and near-IR catalogues, plotted using the same symbols as Figure 1. This CMD is used to supplement the optical selection. The solid black line marks the foreground reddening vector (Schlegel et al. 1998).

Offset sky frames (0.′5 to the east) were interleaved between the science observations in an object (O), sky (S) sequence of: O, S, O, O. The observations were performed with the YJ grating (giving coverage from 1.0 to 1.359μm); estimates of the delivered resolving power for each spectrograph (obtained from the KMOS/esorex pipeline for two arc lines) are listed in Table 1.

In addition to the science observations, a standard set of KMOS calibration frames were obtained consisting of dark, flat and arc-lamp calibrations (with flats and arcs taken at six different rotator angles). A telluric standard star was observed with the arms configured in the science positions, i.e. using the *KMOS_spec_cal_stdstarscipatt* template in which the standard star is observed sequentially through all the IFUs. The observed standard was

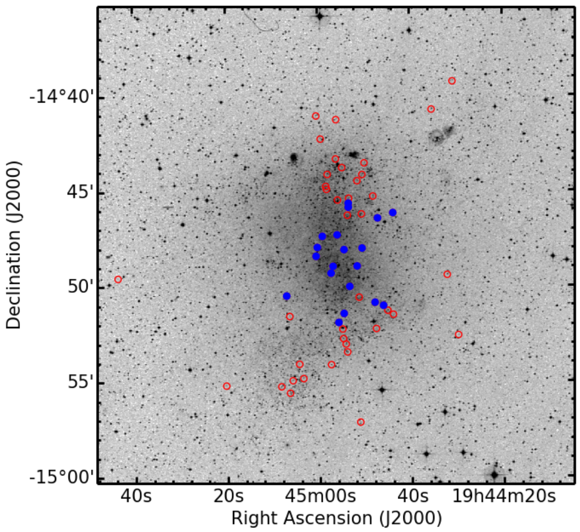

Figure 3. Spatial extent of the KMOS targets over a Digital Sky Survey (DSS) image of NGC 6822. Blue filled circles indicate the locations of the observed red supergiant stars. Red open circles indicate the positions of red supergiant candidates selected using a two-colour selection method (Levesque & Massey 2012).

HIP97618, with a spectral type of B6 III (Houk & Smith-Moore 1988).

A summary of the observed targets is given in Table 2. To perform the analysis to a satisfactory standard, the signal-to-noise (S/N) per resolution element for any given spectrum must be $\gtrsim 100$ (Gazak et al. 2014). We estimated the observed S/N by estimating the source signal in the in the $1.15-1.22\mu$m region over the brightest spatial pixels. The sky signal is estimated from the sky exposures in a region where no strong sky lines are present. The S/N estimated is knowingly an underestimate of the true S/N achieved.

3. DATA REDUCTION

The observations were reduced using the recipes provided by the Software Package for Astronomical Reduction with KMOS (SPARK; Davies et al. 2013). The standard KMOS/esorex routines were used to calibrate and reconstruct the science and standard-star data cubes as outlined by Davies et al. (2013). Sky subtraction was performed using the standard KMOS recipes and telluric correction performed using two different strategies. Throughout the analysis presented in this section all the spectra have been extracted from their respective data cubes using a consistent method (i.e. the optimal extraction method within the pipeline).

3.1. *Three-arm vs 24-arm Telluric Correction*

The standard template for telluric observations with KMOS is to observe a standard star in one IFU in each of the three spectrographs. However, there is an alternative template which allows users to observe a standard star in each of the 24 IFUs. This strategy should provide an optimum telluric correction for the KMOS IFUs but reduces observing efficiency.

A comparison between the two methods in the H-band was given by Davies et al. (2013), who concluded that using the more efficient three-arm method was suitable for most science purposes. However, an equivalent analysis in the YJ-band was not available. To determine if the more rigorous telluric routine is required for our analysis, we observed a telluric standard star (HIP97618) in each of the 24 IFUs. This gave us the data to investigate both telluric correction methods and to directly compare the two results.

We compared the standard star spectrum in each IFU with that used by the pipeline routines for the three-arm template in each of the spectrographs. Figure 4 shows the differences between the standard star spectra across the IFUs, where the differences in the YJ-band are comparable to those in the H-band (cf. Fig.7 from Davies et al. 2013). The qualitative agreement between the IFUs in our region of interest ($1.15 - 1.22\mu$m) is generally very good.

To quantify the difference the two telluric methods would make to our analysis, we performed the steps described in Section 3.2 for both templates. We then used the two sets of reduced science data (reduced with both methods of the telluric correction) to compute stellar parameters for our targets. The results of this comparison are detailed in Section 4.1.

3.2. *Telluric Correction Implementation*

To improve the accuracy of the telluric correction, for both methods mentioned above, we implemented additional recipes beyond those of the KMOS/esorex pipeline. These recipes were employed to account for two effects which could potentially degrade the quality of the telluric correction. The first corrects for any potential shift in wavelength between each science spectrum and its associated telluric standard. The most effective way to implement this is to cross-correlate each pair of science and telluric standard. Any shift between the two spectra is then applied to the telluric standard using a cubic-spline interpolation routine.

The second correction applied is a simple spectral scaling algorithm. This routine corrects for differences in line intensity of the most prominent features common to both the telluric and science spectra. To find the optimal scaling parameter the following formula is used,

$$T_2 = (T_1 + c)/(T_1 - c), \qquad (1)$$

where T_2 is the corrected telluric standard spectrum, T_1 is the initial telluric standard spectrum and c is the scaling parameter.

To determine the required scaling, telluric spectra are computed for $-0.5 < c < 0.5$, in increments of 0.02 (where a perfect value, i.e. no difference in line strength would be $c = 0$). The standard deviation is then computed for each telluric-corrected science spectrum, and the minimum value of the standard-deviation matrix defines the optimum scaling. For this algorithm, only the region of interest for our analysis is considered (i.e. $1.15 - 1.22\mu$m).

The final set of telluric standard spectra, generated using the KMOS/esorex routines and modified using the additional routines described above, are used to correct their respective science observations for the effects of the Earth's atmosphere.

3.3. *Sky Subtraction*

Table 1
Measured velocity resolution and resolving power across each detector.

Det.	IFUs	Ar $\lambda 1.12430\,\mu$m		Ne $\lambda 1.17700\,\mu$m	
		FWHM [km s^{-1}]	R	FWHM [km s^{-1}]	R
1	1-8	85.45 ± 2.67	$3\,511 \pm 110$	88.04 ± 2.67	$3\,408 \pm 103$
2	9-16	80.30 ± 3.05	$3\,736 \pm 142$	82.83 ± 2.48	$3\,622 \pm 108$
3	17-24	101.25 ± 2.99	$2\,963 \pm 87$	103.23 ± 2.73	$2\,906 \pm 77$

Table 2
Summary of VLT-KMOS targets in NGC 6822.

Name	Alt. name	S/N	α (J2000)	δ (J2000)	B	V	R	J	H	K_s	Notes
J194443.81−144610.7	RSG5	223	19:44:43.81	−14:46:10.7	20.83	18.59	17.23	14.16	13.37	13.09	Sample
J194445.98−145102.4	RSG8	120	19:44:45.98	−14:51:02.4	20.91	18.96	17.89	15.53	14.72	14.52	Sample
J194447.13−144627.1	RSG9	94	19:44:47.13	−14:46:27.1	21.30	19.41	18.41	16.13	15.35	15.12	
J194447.81−145052.5	RSG12	211	19:44:47.81	−14:50:52.5	20.74	18.51	17.22	14.37	13.58	13.30	LM12, Sample
J194450.54−144801.6	RSG16	104	19:44:50.54	−14:48:01.6	20.83	18.95	17.97	15.75	14.98	14.79	
J194451.64−144858.0	RSG21	105	19:44:51.64	−14:48:58.0	21.33	19.45	18.32	15.81	14.95	14.72	
J194453.46−144552.6	RSG24	145	19:44:53.46	−14:45:52.6	20.36	18.43	17.38	15.06	14.30	14.08	LM12, Sample
J194453.46−144540.1	RSG25	103	19:44:53.46	−14:45:40.1	20.88	19.14	18.17	15.95	15.16	14.98	LM12, Sample
J194454.46−144806.2	RSG29	201	19:44:54.46	−14:48:06.2	20.56	18.56	17.35	14.43	13.67	13.34	LM12, Sample
J194454.54−145127.1	RSG30	302	19:44:54.54	−14:51:27.1	19.29	17.05	15.86	13.43	12.66	12.42	LM12, Sample
J194455.70−145155.4	RSG34	327	19:44:55.70	−14:51:55.4	19.11	16.91	15.74	13.43	12.70	12.43	LM12, Sample
J194455.93−144719.6	RSG36	100	19:44:55.93	−14:47:19.6	21.43	19.56	18.52	16.14	15.33	15.14	LM12
J194456.86−144858.5	RSG39	106	19:44:56.86	−14:48:58.5	21.05	19.06	18.04	15.81	15.05	14.85	
J194457.31−144920.2	RSG40	284	19:44:57.31	−14:49:20.2	19.69	17.41	16.20	13.52	12.76	12.52	LM12, Sample
J194459.14−144723.9	RSG45	124	19:44:59.14	−14:47:23.9	21.30	19.17	18.05	15.58	14.74	14.50	
J194500.24−144758.9	RSG47	107	19:45:00.24	−14:47:58.9	21.27	19.20	18.10	15.60	14.80	14.57	
J194500.53−144826.5	RSG49	167	19:45:00.53	−14:48:26.5	20.84	18.75	17.51	14.70	13.86	13.61	Sample
J194506.98−145031.1	RSG55	104	19:45:06.98	−14:50:31.1	21.06	19.12	18.06	15.74	14.94	14.78	Sample

Note. — Optical data from Massey et al. (2007), near-IR data from the UKIRT survey (see Sibbons et al. 2012, for details). Targets with the comment 'LM12' are those observed by Levesque & Massey (2012). Targets with the comment 'Sample' are those used for the abundance analysis in this paper.

Initial inspection of the spectra revealed minor residuals from the sky subtraction process. Reducing these cases with the 'sky_tweak' option within the KMOS/esorex reduction pipeline was ineffective to improve the subtraction of these features. Any residual sky subtraction features could potentially influence our results by perturbing the continuum placement within the model fits, which is an important aspect of the fitting process (see Davies et al. submitted; Gazak et al. 2014, for more discussion). Thus, pending a more rigorous treatment of the data (e.g. to take into account the changing spectral resolution across the array), we exclude objects showing residual sky-subtraction features from our analysis. Of the 18 observed targets, 11 were used to derive stellar parameters (as indicated in Table 2).

4. RESULTS

Stellar parameters (metallicity, effective temperature, surface gravity and microturbulence) have been derived using the J-band analysis technique described by Davies et al. (2010) and demonstrated by Davies et al. (submitted) and Gazak et al. (2014). To determine physical parameters, this technique uses a grid of synthetic spectra to fit the observational data. The resolution of the models is determined by the measured resolution from the KMOS/esorex pipeline (Table 1). Model atmospheres were generated using the MARCS code (Gustafsson et al. 2008) where the range of parameters are defined in Table 3. The precision of the models is increased by including departures from LTE in some of the strongest Fe, Ti and Si atomic lines (Bergemann et al. 2012, 2013). The two strong magnesium lines are excluded from the analysis at present as these lines are known to be affected strongly by non-LTE effects (see Figure 5, where the two MgI lines are systematically under- and over-estimated, respectively). The non-LTE line-formation of Mg I lines will be explored by Bergemann et al. (in prep).

Table 3
Model grid ranges used for analysis.

Model Parameter	Min.	Max.	Step size
T_{fit} (K)	3400	4000	100
	4000	4400	200
[Z] (dex)	−1.50	1.00	0.25
log g (cgs)	−1.0	1.0	0.5
ξ (km s^{-1})	1.0	6.0	1.0

4.1. *Telluric Comparison*

We used these SV data to determine which of the two telluric standard methods is most appropriate for our analysis. Table 4 details the stellar parameters derived for each target using both telluric methods and these parameters are compared in Figure 6. The mean difference in metallicity for the two methods is $\Delta[Z] = 0.01 \pm 0.10$. Therefore, for our analysis, there is no significant difference between the two telluric methods.

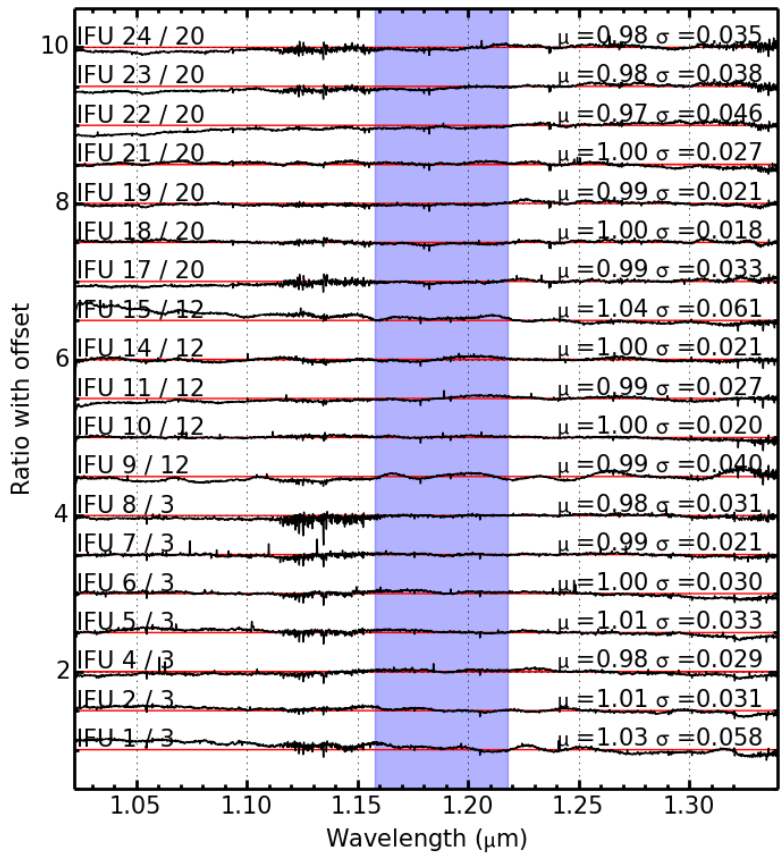

Figure 4. Comparison of J-band spectra of the same standard star in each IFU. The ratio of each spectrum compared to that from the IFU used in the three-arm telluric method is shown, with their respective mean and standard deviation (μ and σ). Red lines indicate $\mu = 1.0$, $\sigma = 0.0$ for each ratio. The blue shaded area signifies the region used in our analysis, within which, the discrepancies between the IFUs are generally small. This is reflected in the standard deviation values when only considering this region. (IFUs 13 and 16 are omitted as no data were taken with these IFUs.)

Table 4
Fit parameters for reductions using the two different telluric methods.

Target	IFU	24 Arm Telluric				3 Arm Telluric			
		T_{fit} (K)	log g	ξ (km s^{-1})	[Z]	T_{fit} (K)	log g	ξ (km s^{-1})	[Z]
RSG5	6	3790 ± 80	−0.0 ± 0.3	3.5 ± 0.4	−0.55 ± 0.18	3860 ± 90	−0.1 ± 0.5	3.5 ± 0.4	−0.61 ± 0.21
RSG8	11	3850 ± 100	0.4 ± 0.5	3.5 ± 0.4	−0.78 ± 0.22	3810 ± 110	0.4 ± 0.5	3.3 ± 0.5	−0.65 ± 0.24
RSG12	12	3880 ± 70	0.0 ± 0.3	4.0 ± 0.4	−0.32 ± 0.16	3880 ± 70	0.0 ± 0.3	4.0 ± 0.4	−0.32 ± 0.16
RSG24	2	3970 ± 60	0.4 ± 0.5	3.9 ± 0.4	−0.58 ± 0.19	3990 ± 80	0.1 ± 0.5	3.8 ± 0.5	−0.56 ± 0.14
RSG25	3	3910 ± 100	0.6 ± 0.5	3.0 ± 0.4	−0.58 ± 0.24	3910 ± 100	0.6 ± 0.5	3.0 ± 0.4	−0.58 ± 0.24
RSG29	4	3980 ± 60	0.1 ± 0.4	3.7 ± 0.4	−0.38 ± 0.16	3990 ± 80	−0.1 ± 0.5	3.6 ± 0.4	−0.44 ± 0.17
RSG30	14	3900 ± 80	−0.3 ± 0.5	3.7 ± 0.4	−0.67 ± 0.16	3850 ± 80	−0.3 ± 0.5	3.5 ± 0.4	−0.59 ± 0.19
RSG34	15	3870 ± 80	−0.4 ± 0.5	4.2 ± 0.5	−0.53 ± 0.19	3850 ± 60	−0.3 ± 0.4	4.3 ± 0.5	−0.49 ± 0.17
RSG40	17	3910 ± 110	−0.5 ± 0.5	3.6 ± 0.5	−0.20 ± 0.21	3880 ± 110	−0.5 ± 0.5	3.6 ± 0.5	−0.15 ± 0.24
RSG49	21	3890 ± 120	0.1 ± 0.5	3.0 ± 0.4	−0.43 ± 0.28	3890 ± 120	0.1 ± 0.5	3.0 ± 0.4	−0.43 ± 0.28
RSG55	18	3810 ± 130	0.4 ± 0.5	2.2 ± 0.4	−0.68 ± 0.31	3740 ± 130	0.4 ± 0.5	2.1 ± 0.5	−0.54 ± 0.41

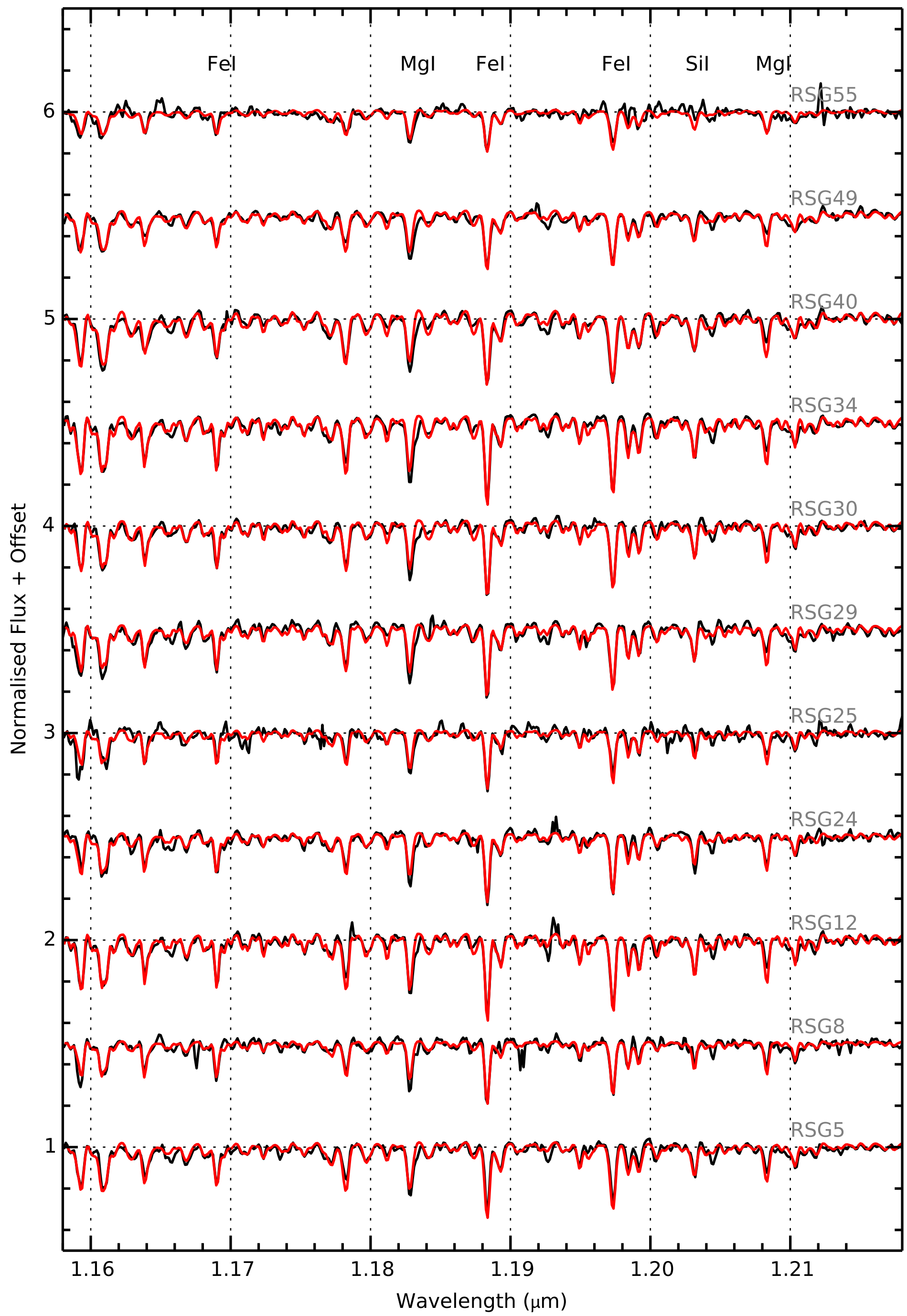

Figure 5. KMOS spectra of the NGC 6822 RSGs and their associated best-fit model spectra (black and red lines, respectively). Some of the main absorption lines are marked.

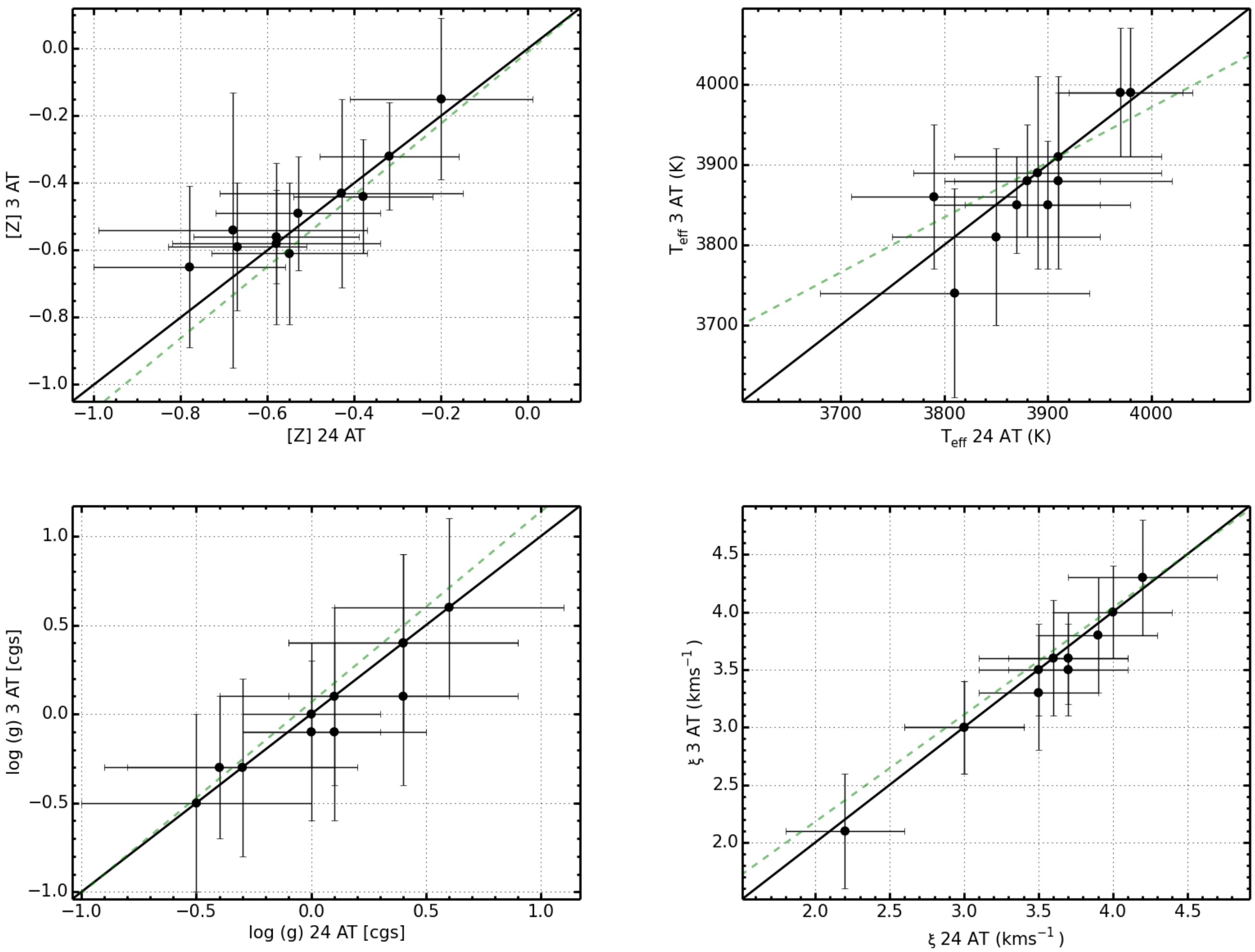

Figure 6. Comparison of the final model parameters using the two different telluric methods. Top left: metallicity ([Z]), mean difference $<\Delta[Z]> \; = 0.04 \pm 0.07$. Top right: effective temperature ($T_{\rm eff}$), mean difference $<\Delta T_{\rm eff}> \; = -14 \pm 42$. Bottom left: surface gravity (log g), mean difference $<\Delta \log g> \; = -0.06 \pm 0.12$. Bottom right: Microturbulence (ξ), mean difference $<\Delta\xi> \; = -0.1 \pm 0.1$. Black solid lines indicate direct correlation between the two methods. Green dashed lines indicates linear best fit to the data. In all cases, the distributions are statistically consistent with a one-to-one ratio (black lines).

4.2. *Stellar Parameters and Metallicity*

Table 4 summarises the derived stellar parameters. For the remainder of this paper, when discussing stellar parameters, we adopt those derived using the 24-arm telluric method (i.e. the left-hand results in Table 4.)

The average metallicity for our sample of 11 RSGs in NGC 6822 is $\bar{Z} = -0.52 \pm 0.21$. This result is in good agreement with the average metallicity derived in NGC 6822 from blue supergiant stars (BSGs; Muschielok et al. 1999; Venn et al. 2001). Excluding the potential outlier (RSG5) from this analysis does not affect the average metallicity measurement.

A direct comparison with metallicities from BSGs is legitimate as the results derived here yield a global metallicity ([Z]) which closely resembles the Fe/H ratio derived from BSGs. While our [Z] measurements are also affected by Si and Ti, we assume [Z] = [Fe/H] for the purposes of our discussion. Likewise, we can compare oxygen abundances (relative to solar) obtained from HII regions as a proxy for [Z] by introducing the solar oxygen abundance $12+\log(\mathrm{O/H})_{\odot}=8.69$ (Asplund et al. 2009) through the relation $[Z]=12+\log(\mathrm{O/H})-8.69$.

The RSG and BSG stages are different evolutionary stages within the life cycle of a massive star, while HII regions are the birth clouds which give rise to the youngest stellar population. As the lifetimes of RSGs and BSGs are $<$ 50Myr, metallicity measurements from these stars are expected to be representative of the metallicities of their birth clouds.

To investigate the spatial distribution of chemical abundances in NGC 6822, in Figure 7 we show the metallicities of our RSGs as a function of radial distance from the centre of the galaxy, as well as the results from Venn et al. (2001) and indicative estimates from Muschielok et al. (1999).

A least-squares fit to the KMOS results reveals a low-significance abundance gradient within the central 1 kpc of NGC 6822 of -0.52 ± 0.35 dex kpc^{-1}. The extrapolated central metallicity from the fit (i.e. at R=0) of $[Z]=-0.30\pm0.15$ derived remains consistent with the average metallicity assuming no gradient.

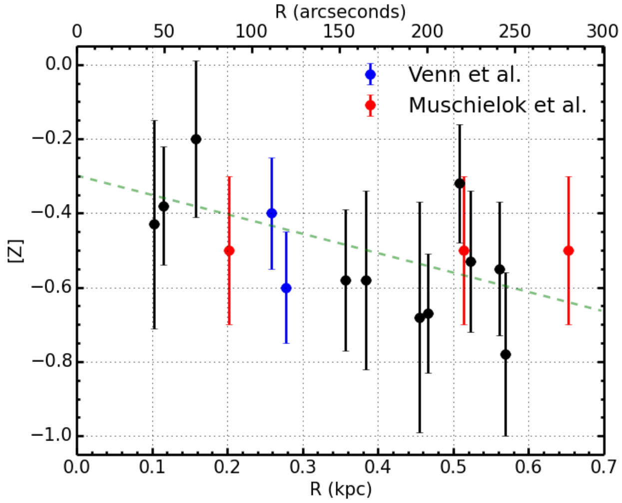

Figure 7. Derived metallicities for 11 RSGs in NGC 6822 shown against their distance from the galaxy centre; the average metallicity is $\bar{Z} = -0.52 \pm 0.21$. A least-squares fit to the KMOS results reveals a low-significance abundance gradient [Z] = $(-0.30 \pm 0.15) + (-0.52 \pm 0.35)R$ with a $\chi^2_{red} = 1.14$. Blue points show the results from two A-type supergiant stars from Venn et al. (2001). Including these results into the fit we obtain a consistent gradient -0.48 ± 0.33 dex kpc^{-1} with an improved $\chi^2_{red} = 1.06$. Red points show the results from three BSG from Muschielok et al. (1999). Results from Muschielok et al. (1999) are not included into the fit as these measurements are qualitative estimates of metallicity. $R_{25} = 460''$ (= 1.12 kpc; McConnachie 2012).

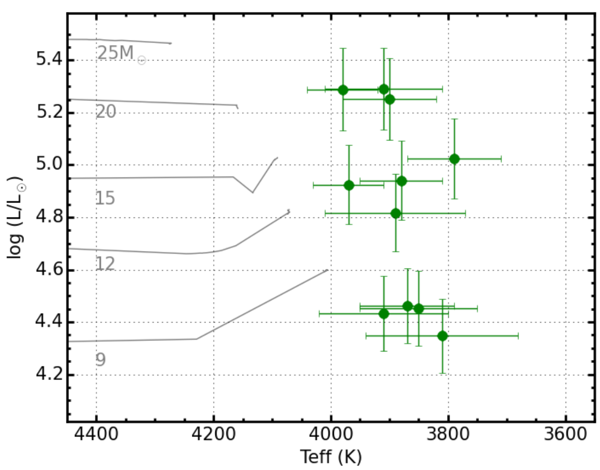

Figure 8. H-R diagram for the 11 RSGs in NGC 6822. Evolutionary tracks including rotation ($v/v_c = 0.4$) for SMC-like metallicity ($Z = 0.002$) are shown in grey, along with their zero-age mass (Georgy et al. 2013). Bolometric corrections are computed using the calibration in Davies et al. (2013). We note that compared to the evolutionary tracks, the observed temperatures of NGC 6822 RSGs are systematically cooler. This is discussed in Section 5.2.

Figure 8 shows the location of RSGs in the Hertzsprung-Russell (H-R) diagram. Bolometric corrections were computed using the calibration in Davies et al. (2013). This figure shows that the temperatures derived using the *J*-band method are systematically cooler than the end of the evolutionary models for $Z = 0.002$ from Georgy et al. (2013). This is discussed in Section 5.2.

5. DISCUSSION

5.1. *Metallicity Measurements*

We find an average metallicity for NGC 6822 of $\bar{Z} = -0.52 \pm 0.21$ which agrees well with the results derived from BSGs (Muschielok et al. 1999; Venn et al. 2001; Przybilla 2002) and HII regions (Lee et al. 2006).

We also find evidence for a low-significance metallicity gradient within the central 1 kpc in NGC 6822 (-0.52 ± 0.35 dex kpc^{-1}; see Figure 7). The gradient derived is consistent with the trend reported in Venn et al. (2001) who derived metallicities of two BSGs and combined that with some of the best available HII region data. The gradient is also consistent with the metallicity gradient derived from a sample of 49 local star-forming galaxies Ho-submitted. Including the results for BSGs from Venn et al. (2001) in our analysis, gives a consistent gradient (-0.48 ± 0.33 dex kpc^{-1}) with a smaller $\chi^2_{red} = 1.06$.

Lee et al. (2006) used 19 HII regions and found no clear evidence for a metallicity gradient. Using a consistent subset of the highest quality HII region data available these authors found a gradient of -0.16 ± 0.05dex kpc^{-1}. Including these results into our analysis degrades the fit and changes the derived gradient significantly (-0.18 ± 0.05 dex kpc^{-1}; $\chi^2_{red} = 1.78$). At this point it is not clear whether the indication of a gradient obtained from the RSGs and BSGs is just an artefact of the small sample size, or indicates a difference with respect to the HII region study.

Comparing our results with previous estimates, Tolstoy et al. (2001) use red giant branch (RGB) stars to estimate the mean metallicity to be [Fe/H] = −0.9 and found a large spread in meatllicity (see Figure 19 in Tolstoy et al. 2001). Sibbons et al. (2012) derived metallicities using a population of asymptotic giant branch (AGB) stars within the central 4 kpc of NGC 6822. They found an average metallicity of [Fe/H] = -1.29 ± 0.07 dex. Likewise Kirby et al. (2013) used spectra of red giant stars within the central 2 kpc and found an average metallicity of [Fe/H] = -1.05 ± 0.49. These authors found no compelling evidence for spatial variations in metallicity. The stellar populations used for these studies are known to be significantly older than the RSGs, therefore, owing to the chemical evolution in the time between the birth of these populations, we expect the measured metallicities to be significantly lower. Additionally, in disc galaxies, we expect a shallower metallicity gradient in these populations as radial motions act to smooth out abundance gradients over time. Therefore it is unsurprising that these authors see no evidence for abundance gradients.

The low metallicity of the young stellar population and the ISM in NGC 6822 can be easily understood as a consequence of the fact that it is a relatively gas rich galaxy with a mass $M_{HI} = 1.38 \times 10^8$ M$_\odot$ (Koribalski et al. 2004) and a total stellar mass of $M_* = 1 \times 10^8$ M$_\odot$ (Weisz et al. 2014). The simple closed-box chemical-evolution model relates the metallicity mass fraction Z(t) at any time to the ratio of stellar to gas mass $\frac{M_*}{M_g}$ through

$$Z(t) = \frac{y}{1-R} \ln\left[1 + \frac{M_*(t)}{M_g(t)}\right], \quad (2)$$

where y is the fraction of metals per stellar mass produced through stellar nucleosynthesis (the so-called yield) and R is the fraction of stellar mass returned to the

ISM through stellar mass-loss. According to Kudritzki et al. (2014, in preparation) the ratio $y/(1-R)$ can be empirically determined from the fact that the metallicity of the young stellar population in the solar neighborhood is solar with a mass fraction $Z_{\odot}$ =0.014 (Nieva & Przybilla 2012). With a solar neighborhood ratio of stellar to gas mass column densities of 4.48 (Wolfire et al. 2003; Bovy & Rix 2013) one then obtains $y/(1-R) = 0.0082 = 0.59Z_{\odot}$ with an uncertainty of 15 percent dominated by the 0.05 dex uncertainty of the metallicity determination of the young population in the solar neighbourhood. Accounting for the presence of helium and metals in the neutral interstellar gas we can turn the observed HI mass in NGC 6822 into a gas mass via $M_g = 1.36\ M_{HI}$ and use the simple closed-box model to predict a metallicity of $[Z] = -0.6 \pm 0.05$, in good agreement with our value obtained from RSG spectroscopy.

As discussed above, the older stellar population of AGB stars has a metallicity roughly 0.7 dex lower than what we measure for the RSGs. In the framework of the simple closed-box model this would correspond to a period in time where the ratio of stellar to gas mass was 0.07 (much lower than the present value of 0.53) and the stellar mass was only $0.19 \times 10^8 M_{\odot}$. The present star-formation rate of NGC 6822 is 0.027 $M_{\odot}yr^{-1}$ (Israel et al. 1996; Cannon et al. 2006; Gratier et al. 2010). At such a high level of star formation it would have taken three Gyr to produce the presently observed stellar mass and to arrive from the average metallicity of the AGB stars to that of the young stellar population (of course, again relying on the simple closed-box model). With a lower star-formation rate it would have taken correspondingly longer.

Given the irregularities present in the morphology of NGC 6822 this galaxy may not be a good example of a closed-box system, however it is remarkable that the closed-box model reproduces the observed metallicity so closely.

5.2. *Temperatures of RSGs*

Effective temperatures have been derived for 11 RSGs from our observed sample in NGC 6822. To date, this represents the fourth data set used to derive stellar parameters in this way and the first with KMOS. The previous three data sets which have been analysed are those of 11 RSGs in PerOB1, a Galactic star cluster (Gazak et al. 2014), nine RSGs in the LMC and 10 RSGs in the SMC (both from Davies et al. submitted). These results span a range of ~0.7 dex in metallicity ranging from $Z=Z_{\odot}$ in PerOB1 to $Z=0.3Z_{\odot}$ in the SMC.

We compare the effective temperatures derived in this study to those of the previous results in different environments. Their distribution is shown as a function of metallicity in Figure 9. Additionally, Figure 10 shows the H-R diagram for the for sets of results. Bolometric corrections for the entire sample are computed using the calibration in Davies et al. (2013).

From these figures, we see no evidence for significant variations in the average temperatures of RSGs with respect to metallicity. This is in contrast to current evolutionary models which display a change of ~450K, for a $M = 15M_{\odot}$ model, over a range of 0.7 dex (Ekström et al. 2012; Georgy et al. 2013).

For solar metallicity, observations in PerOB1 are in good agreement with the models (see Figure 9 in Gazak et al. 2014). However, at SMC-like metallicity, the end-points of the evolutionary models are systematically warmer than the observations. The temperature of the end-points of the evolutionary models of massive stars could depend on the choice of the convective mixing length parameter (Schaller et al. 1992). That the models produce a higher temperature than observed could imply that the choice of a solar-like mixing length parameter does not hold for higher mass stars at lower metallicity.

There is evidence however, that the average spectral

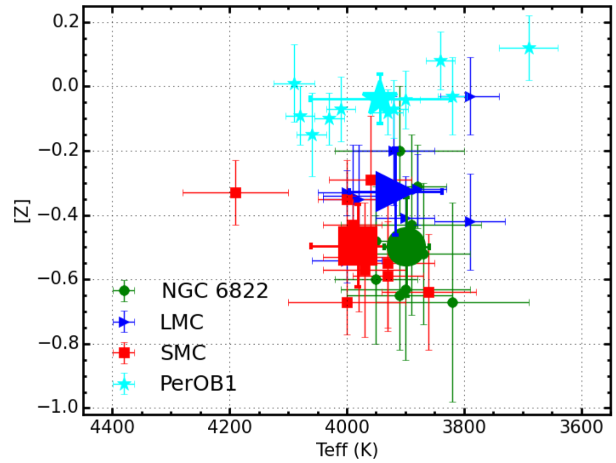

Figure 9. Effective temperatures shown as a function of metallicity for four different data sets using the *J*-band analysis technique. There appears to be no significant evolution in the temperatures of RSGs over a range of 0.7 dex. These results are compiled from the LMC, SMC (blue and red points respectively; Davies et al. submitted), PerOB1 (a Galactic RSG cluster; cyan; Gazak et al. 2014) and NGC 6822 (green). Mean values for each data set are shown as enlarged points in the same style and colour. The x-axis is reversed for comparison with Figure 10.

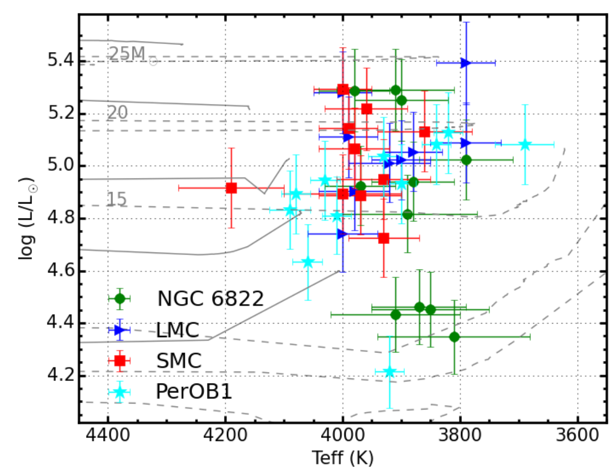

Figure 10. H-R diagram for RSGs in PerOB1 (cyan), LMC (blue), SMC (red) and NGC 6822 (green) which have stellar parameters obtained using the *J*-band method. This figure shows that there appears to be no significant temperature difference between the four studies. Solid grey lines show SMC-like metallicity evolutionary models including rotation (Georgy et al. 2013). Dashed grey lines show solar metallicity evolutionary models including rotation (Ekström et al. 2012).

type of RSGs tends towards an earlier spectral type with decreasing metallicity over this range (Humphreys 1979; Levesque & Massey 2012). We argue that these conclusions are not mutually exclusive. Spectral types are derived for RSGs using the optical TiO band-heads at $\sim 0.65 \mu$m, whereas in this study temperatures are derived using near-IR atomic features (as well as the line-free pseudo-continuum). The strength of TiO bands are dependent upon metallicity which means that the spectral classification for RSGs at a constant temperature will differ (Davies et al. 2013). Therefore, although historically spectral type has been used as a proxy for temperature, this assumption does not provide an accurate picture for RSGs.

6. CONCLUSIONS

KMOS spectroscopy of red supergiant stars (RSGs) in NGC 6822 is presented. The data were telluric corrected in two different ways and the standard 3-arm telluric method is shown to work as effectively (in most cases) as the more time expensive 24-arm telluric method.

Stellar parameters are calculated for 11 RSGs using the *J*-band analysis method outlined in Davies et al. (2010). The average metallicity within NGC 6822 is $\bar{Z} = -0.52 \pm 0.21$, consistent with previous abundance studies of young stars. We find an indication of a metallicity gradient within the central 1 kpc, however with a low significance caused by the small size and limited spatial extent of our RSG sample.

Using a closed-box chemical evolution model, measurements of the young and old stellar populations of NGC 6822 can be explained through chemical evolution. However, while an interesting result, we note that the closed-box model is unlikely to be a good assumption for this galaxy given its morphology. To conclusively assess the presence of a metallicity gradient among the young population within NGC 6822 a larger systematic study of RSGs is needed.

The effective temperatures of RSGs in this study are compared to those of all RSGs analysed in the same way. Using results which span 0.7 dex in metallicity (solar-like to SMC-like) within four galaxies, we find no evidence for a systematic variation in average effective temperature with respect to metallicity. This is in contrast with evolutionary models for which a change in metallicity of 0.7 dex produces a shift in the temperature of RSGs of up to 450K. We argue that an observed shift in average spectral type of RSGs observed over the same metallicity range (0.7 dex) does not imply a shift in average temperature.

These observations were taken as part of the KMOS Science Verification program. With guaranteed time observations we have obtained data for RSGs in NGC 300 and NGC 55 at distances of $\sim$1.9 Mpc, as well as observations of super-star clusters in M 83 and the Antennae galaxy at 4.5 and 20 Mpc respectively. Owing to the fact that RSGs dominate the light output from super-star clusters (Gazak et al. 2013) these clusters can be analysed for abundance estimates in a similar manner (Gazak et al. 2014), which will provide metallicity measurements at distances a factor of 10 larger than using individual RSGs! This work will form the basis of an ambitious general observation proposal to survey a large number of galaxies in the Local Volume, motivated by the twin goals of investigating their abundance patterns, while also calibrating the relationship between galaxy mass and metallicity in the Local Group.

We thank Mike Irwin for providing the photometric catalogue from the WFCAM observations. RPK and JZG acknowledge support by the National Science Foundation under grant AST-1108906

Facilities:, VLT (KMOS).

REFERENCES

Asplund, M., Grevesse, N., Sauval, A. J., & Scott, P. 2009, ARA&A, 47, 481
Battinelli, P., Demers, S., & Kunkel, W. E. 2006, A&A, 451, 99
Bergemann, M., Kudritzki, R.-P., Plez, B., et al. 2012, ApJ, 751, 156
Bergemann, M., Kudritzki, R.-P., Würl, M., et al. 2013, ApJ, 764, 115
Bergemann, M., et al., in prep.
Bovy, J., & Rix, H.-W. 2013, ApJ, 779, 115
Cannon, J. M., Walter, F., Armus, L., et al. 2006, ApJ, 652, 1170
Cioni, M.-R. L., & Habing, H. J. 2005, A&A, 429, 837
Clementini, G., Held, E. V., Baldacci, L., & Rizzi, L. 2003, ApJ, 588, L85
Davies, B., et al., submitted.
Davies, B., Kudritzki, R.-P., & Figer, D. F. 2010, MNRAS, 407, 1203
Davies, B., Kudritzki, R.-P., Plez, B., et al. 2013, ApJ, 767, 3
Davies, R. I., Agudo Berbel, A., Wiezorrek, E., et al. 2013, A&A, 558, A56
de Blok, W. J. G., & Walter, F. 2000, ApJ, 537, L95
de Blok, W. J. G., & Walter, F. 2003, MNRAS, 341, L39
de Blok, W. J. G., & Walter, F. 2006, AJ, 131, 343
Demers, S., Battinelli, P., & Kunkel, W. E. 2006, ApJ, 636, L85
Ekström, S., Georgy, C., Eggenberger, P., et al. 2012, A&A, 537, A146
Evans, C. J., Davies, B., Kudritzki, R.-P., et al. 2011, A&A, 527, A50
Feast, M. W., Whitelock, P. A., Menzies, J. W., & Matsunaga, N. 2012, MNRAS, 421, 2998
Gazak, J. Z., Davies, B., Kudritzki, R., Bergemann, M., & Plez, B. 2014, ApJ, 788, 58
Gazak, J. Z., Davies, B., Bastian, N., et al. 2014, ApJ, 787, 142
Gazak, J. Z., Bastian, N., Kudritzki, R.-P., et al. 2013, MNRAS, 430, L35
Georgy, C., Ekström, S., Eggenberger, P., et al. 2013, A&A, 558, A103
Gratier, P., Braine, J., Rodriguez-Fernandez, N. J., et al. 2010, A&A, 512, A68
Gustafsson, B., Edvardsson, B., Eriksson, K., et al. 2008, A&A, 486, 951
Hernández-Martínez, L., Peña, M., Carigi, L., & García-Rojas, J. 2009, A&A, 505, 1027
Ho, I.-T., et al., submitted
Houk, N., & Smith-Moore, M. 1988, Michigan Catalogue of Two-dimensional Spectral Types for the HD Stars. Volume 4, Declinations -26deg.0 to -12deg.0.. N. Houk, M. Smith-Moore.Department of Astronomy, University of Michigan, Ann Arbor, MI 48109-1090, USA. 14+505 pp. Price US 25.00 (USA, Canada), US 28.00 (Foreign) (1988).,
Humphreys, R. M. 1979, ApJ, 231, 384
Huxor, A. P., Ferguson, A. M. N., Veljanoski, J., Mackey, A. D., & Tanvir, N. R. 2013, MNRAS, 429, 1039
Hwang, N., Lee, M. G., Lee, J. C., et al. 2011, ApJ, 738, 58
Hwang, N., Park, H. S., Lee, M. G., et al. 2014, ApJ, 783, 49
Israel, F. P., Bontekoe, T. R., & Kester, D. J. M. 1996, A&A, 308, 723
Kirby, E. N., Cohen, J. G., Guhathakurta, P., et al. 2013, ApJ, 779, 102
Komiyama, Y., Okamura, S., Yagi, M., et al. 2003, ApJ, 590, L17
Koribalski, B. S., Staveley-Smith, L., Kilborn, V. A., et al. 2004, AJ, 128, 16
Lee, H., Skillman, E. D., & Venn, K. A. 2006, ApJ, 642, 813

Letarte, B., Demers, S., Battinelli, P., & Kunkel, W. E. 2002, AJ, 123, 832
Levesque, E. M., & Massey, P. 2012, AJ, 144, 2
Massey, P. 1998, ApJ, 501, 153
Massey, P., McNeill, R. T., Olsen, K. A. G., et al. 2007, AJ, 134, 2474
McConnachie, A. W. 2012, AJ, 144, 4
Muschielok, B., Kudritzki, R. P., Appenzeller, I., et al. 1999, A&A, 352, L40
Nieva, M.-F., & Przybilla, N. 2012, A&A, 539, A143
Nikolaev, S., & Weinberg, M. D. 2000, ApJ, 542, 804
Pietrzyński, G., Gieren, W., Udalski, A., et al. 2004, AJ, 128, 2815
Przybilla, N., 2002, Thesis, Munich University Observatory, Ludwig-Maximilian-University Munich.
Schaller, G., Schaerer, D., Meynet, G., & Maeder, A. 1992, A&AS, 96, 269
Schlegel, D. J., Finkbeiner, D. P., & Davis, M. 1998, ApJ, 500, 525
Sharples, R., Bender, R., Agudo Berbel, A., et al. 2013, The Messenger, 151, 21
Sibbons, L. F., Ryan, S. G., Cioni, M.-R. L., Irwin, M., & Napiwotzki, R. 2012, A&A, 540, A135
Tolstoy, E., Irwin, M. J., Cole, A. A., et al. 2001, MNRAS, 327, 918
Venn, K. A., Lennon, D. J., Kaufer, A., et al. 2001, ApJ, 547, 765
Wegner, M., & Muschielok, B. 2008, Proc. SPIE, 7019,
Weisz, D. R., Dolphin, A. E., Skillman, E. D., et al. 2014, ApJ, 789, 147
Wolfire, M. G., McKee, C. F., Hollenbach, D., & Tielens, A. G. G. M. 2003, ApJ, 587, 278